Astron. Astrophys. 343, 615–623 (1999)

ASTRONOMY
AND
ASTROPHYSICS

Stability of a flux tube model for prominences

M. Rempel[⋆]**, D. Schmitt, and W. Glatzel**

Universitäts-Sternwarte Göttingen, Geismarlandstrasse 11, D-37083 Göttingen, Germany

Received 12 May 1998 / Accepted 10 December 1998

Abstract. We discuss the stability of a flux tube model for quiescent solar prominences. The main result is that the configurations are stable only up to a critical width (defined as the extension of the central part of the flux tube with prominence matter at low temperatures) of about $1\,000$ km to $3\,000$ km. The dependence of the critical width on the prominence parameters height, temperature, density contrast, external magnetic field, external gas pressure and external temperature is analysed. The normal modes and eigenfrequencies obtained numerically cover the range of observational data for prominence oscillations.

Key words: instabilities – Magnetohydrodynamics (MHD) – Sun: filaments – Sun: magnetic fields – Sun: prominences

1. Introduction

Quiescent solar prominences are cool, dense clouds in the solar corona which are suspended against gravity by the curvature-forces of magnetic fields penetrating them. The lifetimes of quiescent prominences are up to a few month which justifies the theoretical modeling on the basis of mechanical and thermal equilibria.

A local description of the mechanical properties was first given by Kippenhahn & Schlüter (1957), who gave the intuitive picture of a magnetic hammock. In order to get a global model for a prominence it is necessary to extend this local description to a field structure which is rooted down in the solar photosphere. There are mainly two different types of models which are characterized by the directions of the transverse magnetic field in the prominence and the photosphere. The same direction corresponds to the normal polarity models, the opposite direction to the inverse polarity models, where the prominence rests in a current sheet above a X-type neutral point. A model of the latter case was first proposed by Kuperus & Raadu (1974). Observational data gives evidence, that the normal polarity prominences are mainly prominences with heights less than about $30\,000$ km, whereas the higher prominences are of the inverse polarity type (Leroy et al. 1984). Alternatively a prominence can be described by twisted field structures which was modeled by Priest et al. (1989).

Different attempts has been made to include an energy equation. Hood & Anzer (1988) or Steele & Priest (1990) solved the energy equation for a given field line without treating the full mechanical equilibrium. The mechanical and thermal equilibrium was solved consistently by Lerche & Low (1977) for a simplified energy equation or by Milne et al. (1979) for a one-dimensional Kippenhahn-Schlüter model.

Stability investigations performed by Galindo-Trejo & Schindler (1984) and Galindo-Trejo (1987) show the stability of the models developed by Menzel (1951), Dungey (1953), Kippenhahn & Schlüter (1957) and Lerche & Low (1980). DeBruyne & Hood (1993) analysed the stability of the model developed by Hood & Anzer (1990) with help of the energy principle of Bernstein et al. (1958) and showed instability for many cases. Longbottom et al. (1994) give stability conditions for 2D current sheet models. Schutgens (1997a), (1997b) discusses the different influences of the photospheric boundary conditions on prominences of normal and inverse type.

Stability analysis gives also information about possible prominence oscillations. The different modes are discussed on the basis of idealized models by Joarder & Roberts (1992, 1993), Oliver et al. (1993), Oliver & Ballester (1995) and Joarder et al. (1997).

This work is based on a flux tube model for quiescent solar prominences developed first by Ballester & Priest (1989). Degenhardt & Deinzer (1993), Degenhardt (1995) and Cramphorn (1996) extended this model by self-consistently including an energy balance (Schmitt & Degenhardt 1995). A quiescent prominence is modeled as a sequence of static slender flux tubes arranged behind each other and embedded in an isothermal corona as shown in a sketch in Fig. 1. This model belongs to the normal polarity type. The prominence rests as cool, dense plasma in a dip at the summit of the arch like flux tubes which reach out far into the corona and are rooted down in the chromosphere along lines of opposite magnetic polarity. For each flux tube the magnetohydrostatic force equilibrium and an energy balance between radiative losses, heat conduction and coronal heating is solved numerically.

We tested these models for their dynamical stability by applying the stability formalism for thin magnetic flux tubes de-

⋆ *Present address:* Kiepenheuer-Institut für Sonnenphysik, Schöneckstrasse 6, D-79104 Freiburg, Germany
Correspondence to: M. Rempel (mrempel@kis.uni-freiburg.de)

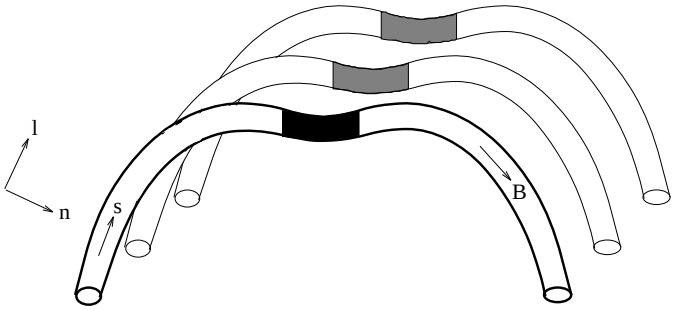

Fig. 1. Sketch of the described model

rived by Schmitt (1995, 1998). He obtained a canonical form of the linear stability equations for slender flux tubes which leads to a self-adjoint force operator for adiabatic perturbations. The analysis yields the conditions for stability and the frequencies of the oscillations in the (neutrally) stable case or growth rates of the disturbances in the unstable case, respectively. The eigenfunctions give hints on the possible instability mechanism. We remark that we only investigate the global stability of an individual thin flux tube of the prominence. The interaction with the environment is given by the lateral pressure balance and a retroaction of the flux tube on the external plasma is neglected.

The eigenvalue problem is solved numerically. As a first step we used a matrix eigenvalue formulation with expansions into fourier modes for a complete spectrum of approximate eigenvalues. For a refined treatment of particular modes we applied the Riccati shooting method (see Gautschy & Glatzel 1990) with adaptive step size integration for the corresponding initial value problem. The use of this method was necessary due to vastly different values of the stability coefficients inside and outside the prominence along the tube. Moreover, we applied the energy principle for a test of the results.

2. Equilibrium models

In the thin flux tube approximation the force balance tangential ($\hat{\boldsymbol{l}}_0$) and normal ($\hat{\boldsymbol{n}}_0$) to the flux tube at $\boldsymbol{r}_0(l_0)$ is given by (the subscript '$_0$' denotes the equilibrium values)

$$\frac{\partial p_0}{\partial l_0} = \varrho_0\, g_0 \left(\hat{\boldsymbol{g}}_0 \cdot \hat{\boldsymbol{l}}_0\right) \tag{1}$$

$$\frac{\kappa_0 B_0^2}{\mu_0} = -\varrho_0 g_0 \left(\hat{\boldsymbol{g}}_0 \cdot \hat{\boldsymbol{n}}_0\right) + \hat{\boldsymbol{n}} \cdot \mathrm{grad}\left(p_0 + \frac{B_0^2}{2\mu_0}\right) \ , \tag{2}$$

where the curvature κ_0 of the flux tube follows from

$$\frac{\partial \hat{\boldsymbol{l}}_0}{\partial l_0} = \kappa_0 \hat{\boldsymbol{n}}_0 \ . \tag{3}$$

The pressure balance in lateral direction is given by

$$\frac{B_0^2}{2\mu_0} + p_0 = \frac{B_e^2}{2\mu_0} + p_e \ , \tag{4}$$

The usual notation of variables is adopted, a subscript '$_e$' denotes external quantities, a hat unit vectors. As equation of state we used the ideal gas law

$$p_0 = \frac{k}{\mu\, m_p}\, \varrho_0 T_0 \ , \tag{5}$$

with the Boltzmann constant k, the mass of the proton m_p and the number of particles per nucleon μ^{-1}. In our models we adopted $\mu = 0.6$ according to the solar chemical composition.

These equations are solved in a cartesian coordinate frame, where the path of the flux tube is given by $(x_0, z_0(x_0))$. The gravitational field g_0 is considered as constant with only a vertical component $\hat{\boldsymbol{g}}_0 = (0, -1)$.

The corona is assumed to be isothermal, leading to

$$p_e = p_{e0} \exp(-z_0/H_e) \ , \tag{6}$$

with the pressure scale height $H_e = kT_e/(\mu m_p g_0)$ and the pressure p_{e0} at the level $z_0 = 0$. This assumption does not consider the temperature decrease towards the photosphere. As the transition layer is very thin, this is a good approximation for our investigation. However, the transition to the photosphere is important for the stability analysis (photospheric boundary condition) which is discussed in detail in Sect. 3.2.

The equilibrium models calculated by Cramphorn and Degenhardt include an energy balance between radiative losses, heat conduction and coronal heating:

$$\mathrm{div}\boldsymbol{q} + L_r - H = 0 \ , \tag{7}$$

where the heat flux $\boldsymbol{q}$ is given by Spitzer (1962)

$$\boldsymbol{q} = -\kappa\, T_0^{5/2}\, \frac{\mathrm{d}T_0}{\mathrm{d}l_0} \hat{\boldsymbol{l}}_{\boldsymbol{0}} \tag{8}$$

with $\kappa = 10^{-11}\mathrm{Wm}^{-1}\mathrm{K}^{-7/2}$. The radiative losses are determined by loss functions given by Hildner (1974), Cox & Tucker (1969) and Kuin & Poland (1991). The coronal heating is chosen as

$$H = h\varrho_0 \tag{9}$$

with a constant h. This energy balance leads to temperature profiles with mainly constant temperatures in the central part of the prominence, a steep gradient in the transition region to the coronal part and a slowly increasing temperature in the corona as shown in Fig. 2.

Using this energy and force balance basic parameters of prominences can be reproduced except for the width which is smaller than observed. Widths bigger than about $500\,\mathrm{km}$ can only be achieved by using very small density contrasts and small central temperatures. But the prominence width has an important influence on the stability, so that the restriction on these models is not very reasonable. In order to analyse wider prominences we worked with a model in which the temperature profile inside the flux tube is prescribed analytically and approximately represents the self-consistent treatment mentioned above. These models are only in magnetohydrostatic force equilibrium and we only investigate the dynamical stability due to

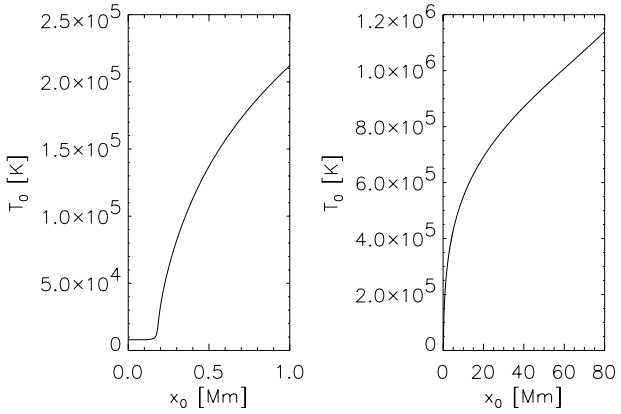

Fig. 2. Temperature profile inside the flux tube for a prominence model with self-consistent energy balance. The central part with low temperatures is shown enlarged in the left plot. The prominence has a width of about 400 km.

adiabatic perturbations. We remark that for the stability analysis only the temperature profiles of the equilibrium model are important and not the energy equations used for obtaining these profiles.

The internal temperature profile of the model is described by

$$T_0(x_0) \;=\; T_{prom} + (T_e - T_{prom}) \cdot \frac{1}{2}\left[1 + \tanh\left(2.65\,\frac{x_0 - b - s}{s}\right)\right] \tag{10}$$

with the half width b of the prominence, the width s of the transition region, the prominence central temperature T_{prom} and the external temperature T_e. This temperature profile shows (for appropriate values of s) the steep gradient in the transition region and is a good approximation for the central part of the prominence. In the coronal part of the flux tube the temperature inside the flux tube is equal to T_e. This is the simplest possible choice but fortunately the results are not strongly dependent on the coronal temperature profile, as long as the temperature is close to the external temperature. This is discussed in detail later.

The influence of an external magnetic field depends mainly on the particular configuration. We used a common arch like potential field

$$B_x = B_{e0}\cos\left(\frac{x_0}{2H_e}\right)\exp\left(-\frac{z_0}{2H_e}\right) \tag{11}$$

$$B_z = -B_{e0}\sin\left(\frac{x_0}{2H_e}\right)\exp\left(-\frac{z_0}{2H_e}\right)\;, \tag{12}$$

where H_e denotes the external pressure scale height and B_{e0} the field strength at the level $z_0 = 0$. This field is a reasonable approximation for the external background field of prominences with normal polarity we want to describe with our model. Another reason for taking this field is the fact that the stability formalism we want to apply was derived for the case without external magnetic field. But it is possible to include this field by a formal substitution we describe in the following lines. A useful property of this field structure is that the field lines are mainly parallel to the path of the flux tube and that the magnetic pressure p_m has the same dependence on height as the external gas pressure p_e. This enables an analytical treatment of the external field by the substitution

$$p_e \;\rightarrow\; \tilde{p}_e = p_e + p_m \tag{13}$$

$$\varrho_e \;\rightarrow\; \tilde{\varrho}_e = \frac{\mu m_p}{kT_e}(p_e + p_m)\;, \tag{14}$$

where $\tilde{p}_e$ and $\tilde{\varrho}_e$ satisfy the equation

$$\mathrm{grad}\,\tilde{p}_e = \tilde{\varrho}_e\, g_0 \left(\hat{\boldsymbol{g}}_0 \cdot \hat{\boldsymbol{l}}_0\right) \tag{15}$$

because of the same height dependence of p_m and p_e. By making use of this property it is possible to write Eqs. (2) and (4) in the form

$$\frac{\kappa_0 B_0^2}{\mu_0} = (\tilde{\varrho}_e - \varrho_0)\, g_0\, (\hat{\boldsymbol{g}}_0 \cdot \hat{\boldsymbol{n}}_0) \tag{16}$$

and

$$\frac{B_0^2}{2\mu_0} + p_0 = \tilde{p}_e\;, \tag{17}$$

which is mathematically equivalent to the case without an external magnetic field, but corresponds to a solution with another effective density contrast between prominence and corona.

The effective central density contrast of the prominence is given by

$$\frac{\varrho_0}{\tilde{\varrho}_e} = \frac{\varrho_0}{\varrho_e}\,\frac{p_{e0}}{p_{e0} + B_{e0}^2/2\mu_0}\;, \tag{18}$$

which is smaller than the real density contrast ϱ_0/ϱ_e and is dependent on the external plasma beta $\beta_e = p_{e0}/(B_{e0}^2/2\mu_0)$. The real density contrast of prominences is about 100. Taking an external magnetic field of about 1–5 G and an external gas pressure of 0.005 Pa, we receive effective density contrasts in the range of 5–50.

Thus using the above described external magnetic field it is sufficient to solve the flux tube equations without an external magnetic field, but keeping in mind that the density contrast is modified by Eq. (18).

If the internal temperature profile, the external plasma beta, external temperature and the (real) density contrast are fixed, the path of the flux tube is unaffected by changing the external gas pressure. The other physical values scale linear with the external gas pressure so that changing the external gas pressure does not produce new solutions. Thus it is possible to reduce the free parameters p_{e0}, B_{e0} and $\varrho_0/\varrho_e(x_0 = 0)$ of the model in the following way:

$$\left.\begin{array}{l} p_{e0} \\ B_{e0} \\ \varrho_0/\varrho_e \end{array}\right\} \rightarrow \beta_e \left.\right\} \rightarrow \varrho_0/\tilde{\varrho}_e$$

The other free parameters are:

– external temperature: T_e

– internal temperature profile: T_{prom}, b, s
– height of prominence: $z_0(x_0 = 0)$

For solving the equations in the cartesian coordinates the following relations are useful. As independent variable we use the horizontal distance x_0, related to the arclength l_0 and height z_0 by $\mathrm{d}{l_0}^2 = \mathrm{d}{x_0}^2 + \mathrm{d}{z_0}^2$.

In the cartesian coordinate frame we get for the Frénet basis ($' = \mathrm{d}/\mathrm{d}x_0$)

$$\hat{\boldsymbol{l}}_0 = \frac{(1, z_0')}{\sqrt{1 + z_0'^2}} \qquad \text{and} \qquad \hat{\boldsymbol{n}}_0 = \frac{(-z_0', 1)}{\sqrt{1 + z_0'^2}} \; . \tag{19}$$

The curvature of the flux tube is given by

$$\kappa_0 = \frac{z_0''}{(1 + z_0'^2)^{3/2}} \; . \tag{20}$$

Using these expressions, Eqs. (1) and (16) can be written as

$$p_0' = -\varrho_0 g_0 z_0' \tag{21}$$

and

$$z_0'' = \frac{1}{2}\left(1 + z_0'^2\right) \frac{1}{\tilde{p}_e - p_0} \left(\varrho_0 - \tilde{\varrho_e}\right) g_0 \tag{22}$$

Using Eqs. (5), (6) and (10) these equations can be integrated with standard routines for ODE's.

A typical prominence model is shown in Fig. 3. Pressure and density profiles of the central part are shown on an enlarged scale. Note that the density contrast inside the flux tube is larger than the density contrast between the prominence and the external corona.

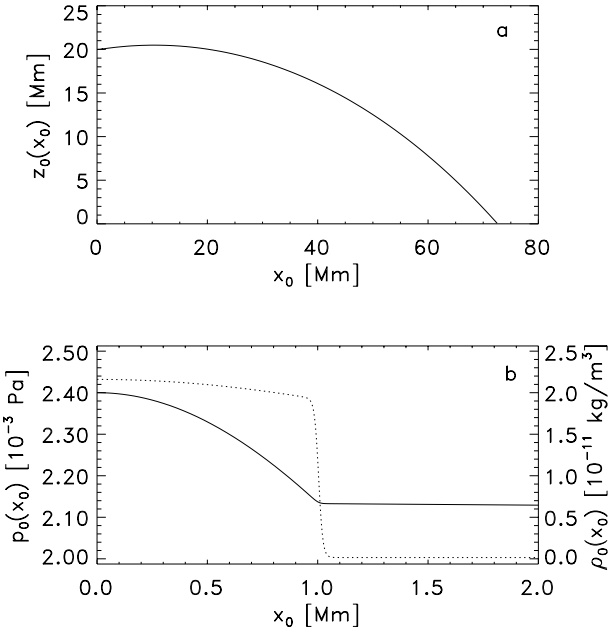

Fig. 3a and b. Equilibrium model for a typical prominence with a prescribed temperature profile. The height is 20 000 km, the width 2 000 km, the central temperature 8 000 K and the effective density contrast between prominence and corona 10. The prominence is embedded in an isothermal corona of 10^6 K. **a** Path of the flux tube. The cool and dense prominence matter rests in the dip at the very center. **b** Pressure (solid line, left axis) and density (dotted line, right axis) profile, enlarged.

3. Stability analysis

3.1. Global stability analysis

The stability analysis is done in terms of the Lagrangian displacement $\boldsymbol{\xi}$ expressed in the Frenet basis vectors as

$$\begin{aligned} \boldsymbol{\xi}(l_0, t) &= \boldsymbol{r}(l, t) - \boldsymbol{r_0}(l_0, t) \\ &= \eta(l_0, t)\, \hat{\boldsymbol{l}}_0 + \varepsilon(l_0, t)\, \hat{\boldsymbol{n}}_0 + \zeta(l_0, t)\, \hat{\boldsymbol{b}}_0 \; , \end{aligned} \tag{23}$$

with the unperturbed arclength l_0, the equilibrium location $\boldsymbol{r}_0$ and the Lagrangian displacement components η, ε and ζ in the tangential direction $\hat{\boldsymbol{l}}_0$, the normal direction $\hat{\boldsymbol{n}}_0$ and the binormal direction $\hat{\boldsymbol{b}}_0$ of the unperturbed flux tube, respectively.

Linearisation of the time dependent thin flux tube equations with respect to $\boldsymbol{\xi}$ and separation of the time dependence as

$$\boldsymbol{\xi}(l_0, t) = e^{i\omega t}\, \boldsymbol{\xi}(l_0) \tag{24}$$

results in the eigenvalue equation ($' = \mathrm{d}/\mathrm{d}l_0$)

$$-\omega^2 \mathcal{P} \begin{pmatrix} \eta \\ \varepsilon \end{pmatrix} = \mathcal{F} \begin{pmatrix} \eta \\ \varepsilon \end{pmatrix} = \begin{pmatrix} \mathcal{A}\,\varepsilon + \mathcal{B}\varepsilon' + \mathcal{C}\,\eta + (\mathcal{E}\eta')' \\ \mathcal{A}\,\eta - (\mathcal{B}\,\eta)' + \mathcal{H}\,\varepsilon + (\mathcal{J}\varepsilon')' \end{pmatrix} \tag{25}$$

for the tangential and normal components. The decoupled binormal component of the perturbation equation yields *stable* Alfvén waves running along the flux tube. $\mathcal{F}$ is a differential operator of second order whose coefficients $\mathcal{A}$, $\mathcal{B}$,... are functions of the unperturbed arclength l_0. For details see Schmitt (1995, 1998). For later application it is useful to transform the independent variable of Eq. (25) from the arclength l_0 to the horizontal distance x_0. Except for the redefinition $' = \mathrm{d}/\mathrm{d}x_0$ Eq. (25) remains unaltered. The coefficients are given in detail in the Appendix. Using the equilibrium model shown in Fig. 3 we obtain coefficients with steep gradients in the prominence-corona transition region and largely constant values in the prominence and coronal part of the flux tube Fig. 4.

It can be shown that the operator $\mathcal{F}$ is self-adjoint thus yielding only real eigenvalues ω^2. The equilibrium is stable, if all eigenvalues ω^2 are positive, and unstable, if at least one eigenvalue exists with $\omega^2 < 0$.

As a consequence of the self-adjointness of $\mathcal{F}$ it is possible to define the change of the potential energy due to perturbations as

$$\delta W = -\frac{1}{2} \int \boldsymbol{\xi}^*\, \mathcal{F}\,(\boldsymbol{\xi})\, \mathrm{d}x_0 \; . \tag{26}$$

Stability corresponds to $\delta W > 0$ for all perturbations and instability prevails if at least one perturbation exists with $\delta W < 0$ (energy principle). Using Eq. (25) yields

$$\begin{aligned} \delta W \;=\; -\frac{1}{2} \int_0^{x_{end}} \big[&\mathcal{A}\,(\eta^*\varepsilon + \eta\varepsilon^*) + \mathcal{B}\left(\eta^*\varepsilon' + \eta\varepsilon^{*\prime}\right) + \\ &\mathcal{C}\eta^*\eta + \mathcal{H}\varepsilon^*\varepsilon - \mathcal{E}\eta^{*\prime}\eta' - \mathcal{J}\varepsilon^{*\prime}\varepsilon' \big]\, \mathrm{d}x_0 \; . \end{aligned} \tag{27}$$

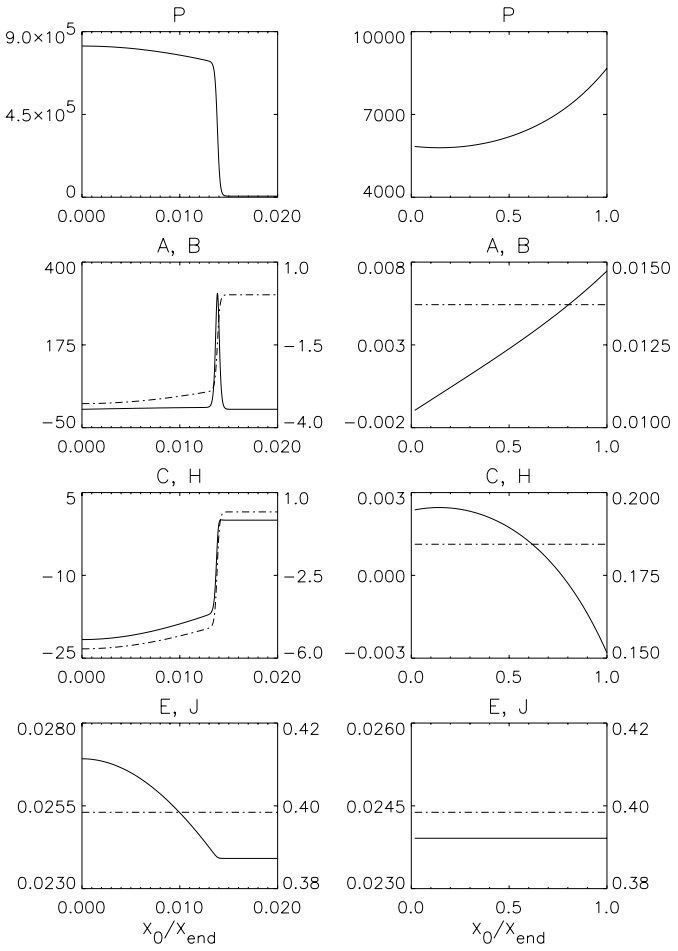

Fig. 4. Coefficients of the stability equation for a typical model. The first coefficient corresponds to a solid line and the left ordinate, the second coefficient to a dash-dotted line and the right ordinate, respectively. The unperturbed horizontal distance x_0 is normalized to its maximum value. The small inner part with the prominence and the sharp interface to the corona is shown in the left diagrams, the large part of the arch through the corona in the right diagrams.

with appropriate boundary conditions (see below) at the end points $x_0 = 0$ and $x_0 = x_{end}$ of the flux tube. If $\boldsymbol{\xi}$ is an eigenfunction we have the relation

$$\delta W = \omega^2 \frac{1}{2} \int_0^{x_{end}} \mathcal{P} \left(\eta^* \eta + \varepsilon^* \varepsilon \right) \, \mathrm{d}x_0 \, , \tag{28}$$

which can be used to test the numerically obtained eigenfunctions and eigenvalues by a simple integration.

3.2. Boundary conditions and eigenfunctions

For solving the eigenvalue problem, boundary conditions have to be specified. The symmetry of the equilibrium model causes a symmetry of the coefficients with respect to the center of the prominence. The coefficient $\mathcal{A}$ is antisymmetric, the other coefficients are symmetric. The structure of Eq. (25) allows for two different symmetries of the eigenfunctions with respect to $x_0 = 0$:

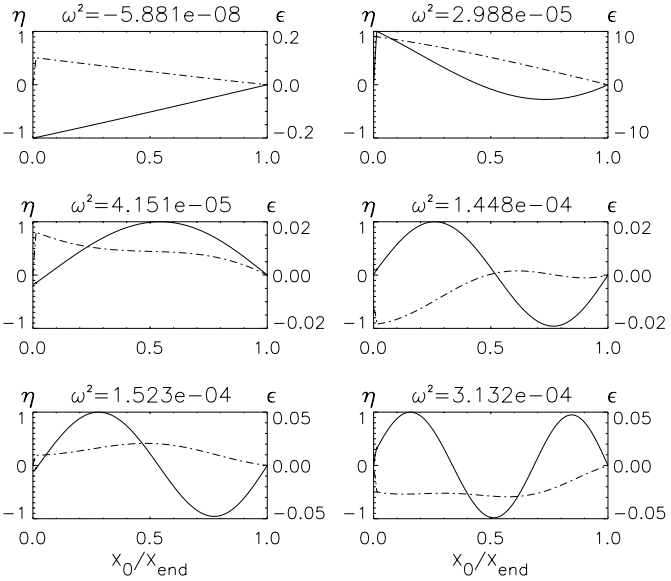

Fig. 5. Eigenfunctions and eigenvalues of the first six eigensolutions for the boundary conditions $\eta'(0) = \varepsilon(0) = 0$ (antisymmetric perturbation) on the left and $\eta(0) = \varepsilon'(0) = 0$ (symmetric perturbation) on the right. Tangential displacements η correspond to solid lines and the left ordinate, normal displacements ε to dash-dotted lines and the right ordinate, respectively. Eigenfunctions are normalized by the maximum of $|\eta|$, x_0 by its maximum value.

(i) η symmetric, ε antisymmetric = antisymmetric perturbation
(ii) ε symmetric, η antisymmetric = symmetric perturbation

As a consequence, it is sufficient to consider only one half of the flux tube and to use the boundary conditions

(i) $\eta'(0) = 0, \varepsilon(0) = 0$
(ii) $\eta(0) = 0, \varepsilon'(0) = 0$

at the center $x_0 = 0$ of the prominence. We assume that the foot point of the arch $x_0 = x_{end}$ is kept fixed in the photosphere of the sun, which implies the boundary condition $\varepsilon(x_{end}) = 0$ for the normal component of the Lagrangian displacement. The tangential component does not need to vanish because a plasma flow along the flux tube induced by the perturbation shall not be excluded. However, taking into account the increase of density in the photosphere, which causes a decrease of any flow speed, the fixed boundary condition $\eta(x_{end}) = 0$ leads to similar results. We checked this numerically by modeling the transition from the corona to the photosphere and solving the eigenvalue problem with the less restrictive condition $\eta'(x_{end}) = 0$. No significant difference was found.

The effect of line-tying on the stability of coronal magnetic fields is discussed in detail by Hood (1986) and Van der Linden et al. (1994).

The first six eigenfunctions together with their eigenvalues are shown in Fig. 5. Note the steep decrease of the normal displacement ε and the tangential displacement η near the origin for the antisymmetric and symmetric fundamental mode, respectively, displayed on an appropriate scale in Fig. 6. It is

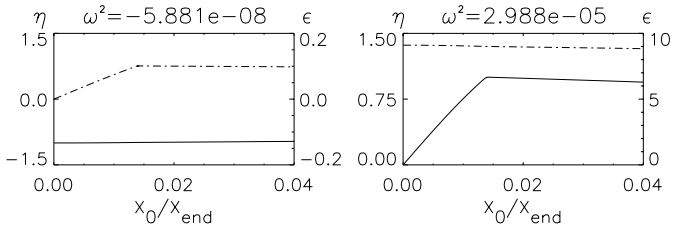

Fig. 6. Enlarged presentation of the first two eigenmodes, which shows the sharp decrease of the normal (antisymmetric mode) and tangential (symmetric mode) displacements at the center. It is caused by the large density and temperature differences between prominence and coronal matter along the flux tube and the associated changes of the coefficients shown in Fig. 4.

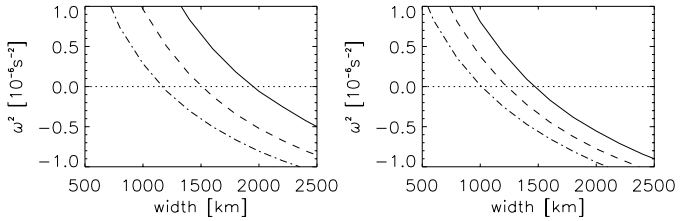

Fig. 7. Variation of the smallest eigenvalue with the prominence width for the effective density contrasts 10 (solid), 30 (dashed) and 50 (dash-dotted). The left graph corresponds to a prominence with a height of 20 000 km, the right to a prominence with a height of 40 000 km. The central prominence temperature is 8 000 K, the external corona temperature 10^6 K.

conspicuous that in all models only the eigenvalue of the antisymmetric fundamental mode with $\eta'(0) = 0$, $\varepsilon(0) = 0$ is very small compared to the other eigenvalues and may become negative, which implies instability. Thus only the sign of this eigenvalue is important for the stability of the configuration. In the following section we discuss the dependence on the different prominence parameters of this eigenvalue.

3.3. Results

The variation of the smallest eigenvalue ω^2 as a function of the different model parameters

- height of the prominence
- width of the prominence
- effective central density contrast of the prominence
- central temperature
- external temperature

is investigated in order to study their influence on the stability of the configuration. For this purpose, different prominence models have been considered, where only one parameter was varied and the other parameters were kept fixed.

The variation of the smallest eigenvalue as a function of height, width and effective density contrast for prominences with a central temperature of 8 000 K and a corona temperature of 10^6 K is shown in Fig. 7. From Fig. 7 we deduce the tendency that an increase of the height and the effective density contrast causes a decrease of the critical width at which the prominence

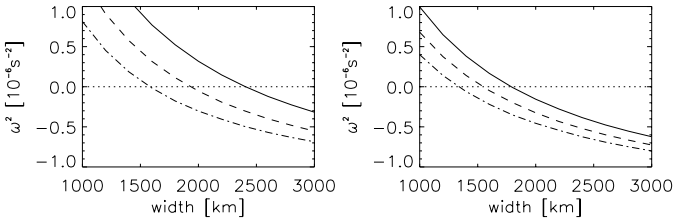

Fig. 8. The same quantities as shown in Fig. 7., but for an external temperature of $1.5 \cdot 10^6$ K.

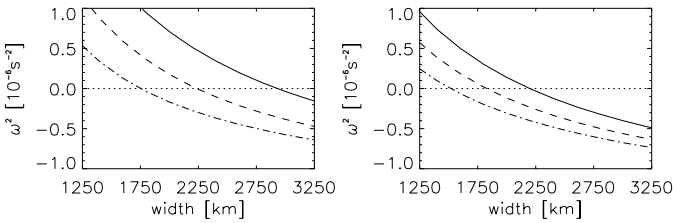

Fig. 9. The same quantities as shown in Fig. 7., but for an external temperature of $1.5 \cdot 10^6$ K and a central temperature of 10 000 K.

becomes unstable. The loss of stability with increasing height corresponds to the observational fact that prominences with normal polarity are usually observed at lower heights.

Fig. 8 is the counterpart of Fig. 7 for a prominence embedded in a corona of $1.5 \cdot 10^6$ K. A comparison with Fig. 7 shows the stabilizing effect of increasing the coronal temperature. This effect is correlated to the destabilization by increasing the height because the coronal part of the prominence solution is determined by the external pressure scale height. Thus an increase of temperature (and pressure scale height) is equivalent to a decrease of the prominence height. A similar result is obtained by increasing the central temperature of the prominence.

In Fig. 9 the variation of the eigenvalues with width and effective density contrast is shown for a prominence with a central temperature of 10 000 K, embedded in a $1.5 \cdot 10^6$ K corona. Compared to Fig. 8 the critical widths are increased up to about 3 000 km in the model with the effective density contrast of 10.

Note that these figures contain the full information of including an external magnetic field as described above. The connection between (real) density contrast, external magnetic field strength and effective density contrast is given by Eq. (18) which shows that the effective density contrast decreases with increasing field strength. Accordingly, (see the results displayed in Figs. 7, 8 and 9) an external magnetic field has a stabilizing effect. These arguments hold only up to a critical field strength because for $\varrho_0 < \tilde{\varrho}_e$ the central dip of the flux loop vanishes and inside the flux tube a density inversion will occur. Rayleigh-Taylor instability, however, is not allowed for by our one-dimensional stability formalism.

If an external magnetic field is included, a prominence model with a central temperature of 10 000 K, an external temperature of $1.5 \cdot 10^6$ K and a density contrast of about 100 can be stable up to a width of 3 000 km if we use $\beta_e \approx 0.1$.

The temperature profile we used is a very good approximation for the central part of the prominence. In the coronal part

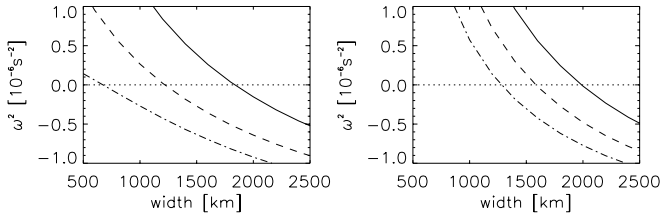

Fig. 10. Variation of the smallest eigenvalue with the prominence width for the effective density contrasts 10 (solid), 30 (dashed) and 50 (dash-dotted). The height is in both plots 20 000 km, the central prominence temperature is 8 000 K and the external corona temperature 10^6 K. The left graph corresponds to a prominence with a temperature of $T = 0.5T_e$ and the right graph corresponds to a prominence with a temperature of $T = 1.5T_e$ in the coronal part of the flux tube.

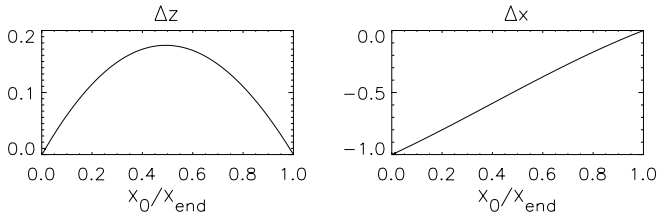

Fig. 11. Vertical and horizontal displacements Δz and Δx of the unstable mode.

of the flux tube are other profiles than $T = T_e$ possible. In order to demonstrate that the temperature in the coronal part does not affect the stability strongly, we present the results obtained with temperature profiles, having coronal values $T = 0.5T_e$ and $T = 1.5T_e$ (Fig. 10). Comparison of the left graph of Fig. 7 with Fig. 10 shows that changing the temperature only affects the critical width of models with a high effective density contrast. Decreasing the temperature in the coronal part of the flux tube means decreasing the internal pressure scale height, leading to an increasing gas pressure (and internal plasma beta) inside the flux tube towards the foot points. This can only affect the stability if the internal plasma beta is sufficiently high enough which is only the case in models with high effective density contrast. But the models with low effective density contrasts are more reasonable if an external magnetic field is included. This means that our restriction to the prescribed temperature profile is a good approximation to more realistic temperature profiles as long as we only consider the dynamical stability.

As mentioned above, changing the external gas pressure (keeping the internal temperature profile, the external plasma beta, external temperature and the (real) density contrast fixed) leads to solutions with the same path but rescaled profiles of pressure and density inside and outside the flux tube. It can also be shown that all coefficients of Eq. (25) have the same dependence on the external pressure, which thus has no effect on the linear eigenvalue problem.

So far we presented the stability analysis for a simplified flux tube model in which we prescribed the temperature profile. As mentioned above the models of Degenhardt (1995) and Cramphorn (1996) have small widths (lower than 500 km) and thus show no instabilities consistent with the results discussed here. The polytropic model of Degenhardt & Deinzer (1993) is found to be unstable.

3.4. Interpretation of the instability

In order to get an intuitive idea of the instability, it is useful to transform the eigenfunctions back into cartesian coordinates. For the eigensolution with the smallest eigenvalue the vertical and horizontal displacements of the flux tube Δx and Δz are shown in Fig. 11.

Obviously the central part of the prominence moves only horizontally (here to the left), whereas the coronal part moves down on the left side and up on the right side. The main point is the fact that the dense plasma of the prominence does not need to flow upward against gravity in order to flow out of the central dip. If this instability occurs, the plasma flows horizontally at $x_0 = 0$ without changing its potential energy.

3.5. Oscillations of prominences

Although we are primarily interested in stability considerations, the analysis also provides a variety of oscillatory modes. Oscillations of prominences have recently received much attention, both observationally and theoretically. Observational data of prominences show long-term oscillations with periods of about 50–80 min and short-term oscillations with periods of about 3–15 min (Tandberg-Hanssen 1995, Sütterlin et al. 1997). A classification of the modes has been achieved on the basis of idealized models by Joarder & Roberts (1992, 1993), Oliver et al. (1993), Oliver & Ballester (1995) and Joarder et al. (1997). In the stable case the smallest eigenvalue of our models corresponds to periods larger than 40 min. The next two oscillations are in the range of about 15–20 min and the higher order oscillations have periods below 10 min. Our modes can be compared to the modes classified by Oliver et al. They distinguish between kink and sausage modes, which correspond to our antisymmetric and symmetric modes. Comparing eigenfunctions and eigenvalues there is a close correspondence between their hybrid slow (mainly horizontal motion) and our antisymmetric fundamental mode. These modes can be observed in prominences at the limb because of their dominating horizontal motion. Binormal displacements of the flux tube correspond to Alfvén modes.

We note that the inertia of the external plasma accelerated by the moving flux tube influences the eigenfrequencies. The exact description of this effect is still under controversial debate (Moreno-Insertis et al. 1996). As long as this effect is parametrized as an enhanced inertia in the normal component of Eq. (25) (Spruit 1981) this leads only to longer oscillation periods, but does not change the sign of the eigenvalues ω^2. This can be proven in the following way: The left hand side of Eq. (25) is modified by the substitution $\varepsilon \rightarrow \mu\varepsilon$ whereas the right hand side remains unaltered. Thus Eq. (27) which determines the sign of ω^2 remains unaltered, too. Spruit introduced $\mu = 1 + \varrho_e/\varrho_0$ assuming a potential flow around the tube.

4. Conclusions

Our stability analysis has shown a flux tube model for quiescent prominences to be stable up to a critical width in the range of 1 000–3 000 km. Increasing the central and external temperature and decreasing the height and the effective density contrast results in an increase of the critical width. The effective density contrast Eq. (18) contains the influence of the real density contrast, the external magnetic field and the external gas pressure. Decreasing the real density contrast and the external plasma beta stabilizes the prominence.

The critical widths we obtained are too small compared to observational data showing typical widths in the range of 5 000 km to 15 000 km.

The periods of the oscillations for stable models are in good agreement with observed prominence oscillations.

The thin flux tube approximation represents an extreme of modeling solar prominences. Useful to describe fibril structures along the magnetic field lines it is an oversimplification when a whole prominence is to be described. Another extreme is the description with a continuous magnetic field, where the global stability analysis is more complicated than in the case of flux tubes. We found an external field to have a stabilizing effect on flux tube models. However, in contrast to a model with a continuous magnetic field, an interaction between the flux tube and the external plasma is not considered in the thin flux tube approximation. Thus it is interesting to compare our results with the stability of such a model. DeBruyne & Hood (1993) analysed the stability of the prominence model developed by Hood & Anzer (1990), which is the "continuous counterpart" of our flux tube model. They found stability for prominences with reasonable widths of 4 000–6 000 km only below a height of about 7 000 km. Using the parameters of their most stable models and taking into account that they adopted $\mu = 1$ inside the prominence and $\mu = 0.6$ in the corona, we obtain a critical width of only about 2 700 km for a height of 7 000 km in our models. This shows that the coupling of the whole field in a continuous model stabilizes the configuration. This can be understood intuitively on the basis of Fig. 11. The vertical displacement would cause a compression (on the left side) or a decompression (on the right side) of external field lines resulting in an increase or a decrease of the magnetic pressure, thus implying an additional restoring force, which stabilizes the configuration.

In Sect. 2 we showed that it is not possible to explain the observed prominence widths in terms of an equilibrium model which makes use of the thermal equilibrium described by Eq. (7). The stability analysis we presented here is based on equilibrium models which exclude the thermal equilibrium in order to be able to describe prominences with realistic widths by using temperature profiles with reasonable prominence properties. As the stability analysis is only dependent on the temperature profiles and not on the thermal equilibrium which is used to determine these profiles, our results give strong restrictions for the possible widths in flux tube models. There may exist thermal equilibria which allow for wider prominences. But if the widths exceed the critical values presented here, the dynamical stability gives the stronger restriction on the prominence width.

Acknowledgements. The authors would like to thank C. Cramphorn and U. Degenhardt for making their equilibrium models and their experience available to them.

Appendix A: coefficients of the stability equation

The coefficients of the stability equation (25) are determined by the equilibrium model (subscript "0") and thus are functions of the unperturbed arclength l_0 or alternatively of the unperturbed horizontal distance x_0. In the latter case they read in detail:

$$\mathcal{A} = \frac{\varrho_0 A_0}{\left(1+z_0'^2\right)^{3/2}} \left\{ -c_T^2 \left(z_0''' - \frac{3 z_0' z_0''^2}{1+z_0'^2} \right) + z_0' z_0'' g_0 \cdot \left(1 - \frac{\varrho_e}{\varrho_0} \right) \frac{c_T^2}{v_A^2} - z_0'' \left(\frac{\varrho_0'}{\varrho_0} c_T^2 + c_T^{2\,\prime} \right) + \left(1+z_0'^2\right) g_0 \cdot \left[\frac{\varrho_e}{\varrho_0} \frac{g_0 z_0'}{c_S^2 + v_A^2} + \varrho_0^{-1} \left(\frac{c_T^2}{v_A^2} \varrho_e \right)' \right] \right\} \quad \text{(A1)}$$

$$\mathcal{B} = -\frac{\varrho_0 A_0 c_T^2}{\left(1+z_0'^2\right)^{3/2}} \left[2 z_0'' + \frac{g_0}{c_S^2} \left(1+z_0'^2\right) \right] \quad \text{(A2)}$$

$$\mathcal{C} = \frac{\varrho_0 A_0 g_0}{\left(1+z_0'^2\right)^{1/2}} \left\{ z_0' \left[\frac{\varrho_e}{\varrho_0} \frac{g_0 z_0'}{c_S^2 + v_A^2} + \varrho_0^{-1} \left(\frac{c_T^2}{v_A^2} \varrho_e \right)' \right] - \frac{z_0''}{1+z_0'^2} \left(1 - \frac{c_T^2}{v_A^2} \frac{\varrho_e}{\varrho_0} \right) \right\} \quad \text{(A3)}$$

$$\mathcal{E} = \frac{\varrho_0 A_0 c_T^2}{\left(1+z_0'^2\right)^{1/2}} \quad \text{(A4)}$$

$$\mathcal{H} = \frac{\varrho_0 A_0}{\left(1+z_0'^2\right)^{3/2}} \left[\frac{z_0''^2}{1+z_0'^2} \frac{v_A^2 \left(v_A^2 - c_S^2\right)}{v_A^2 + c_S^2} - z_0'' g_0 \cdot \left(1 + 2\frac{\varrho_e}{\varrho_0} \right) \frac{c_T^2}{c_S^2} + \left(1+z_0'^2\right) g_0 \frac{\varrho_e}{\varrho_0} \cdot \left(\frac{g_0}{c_S^2 + v_A^2} - H_{\varrho_e}^{-1} \right) \right] \quad \text{(A5)}$$

$$\mathcal{J} = \frac{\varrho_0 A_0 v_A^2}{\left(1+z_0'^2\right)^{1/2}} \quad \text{(A6)}$$

$$\mathcal{P} = \varrho_0 A_0 \left(1+z_0'^2\right)^{1/2} \quad \text{(A7)}$$

with the path of the flux tube $z_0(x_0)$, $' = \mathrm{d}/\mathrm{d}x_0$, the cross-section A_0, the sound speed $c_S = (\gamma p_0/\varrho_0)^{1/2}$, the Alfvén speed $v_A = B_0/(\mu_0 \varrho_0)^{1/2}$ and the tube speed c_T, given by $c_T^2 = (c_S^2\, v_A^2)/(c_S^2 + v_A^2)$. The subscript 'e' corresponds to the external plasma. H_{ϱ_e} denotes the density scale height, given by $H_{\varrho_e}^{-1} = -d \ln \varrho_e / dz_0$. Note that $\mathcal{J}$ is a constant.

References

Ballester J.L., Priest E.R., 1989, A&A 225, 213
Bernstein I.B., Frieman E.A., Kruskal M.D., Kulsrud R.M., 1958, Proc. Roy. Soc. London A244, 17

Cox D.P., Tucker W.H., 1969, ApJ 157, 1157
Cramphorn C., 1996, Diplomarbeit, Univ. Göttingen
DeBruyne, Hood A.W., 1993, Solar Phys. 147, 97
Degenhardt U., 1995, Dissertation, Univ. Göttingen
Degenhardt U., Deinzer W., 1993, A&A 278, 288
Dungey J.W., 1953, MNRAS 113, 180
Galindo-Trejo J., Schindler K., 1984, ApJ 277, 422
Galindo-Trejo J., 1987, Solar Phys. 108, 265
Gautschy A., Glatzel W., 1990, MNRAS 245, 154
Hood A.W., 1986, Solar Phys. 105, 307
Hood A.W., Anzer U., 1988, Solar Phys. 115, 61
Hood A.W., Anzer U., 1990, Solar Phys. 126, 117
Hildner E., 1974, Solar Phys. 35, 123
Joarder P.S., Roberts B., 1992, A&A 261, 625
Joarder P.S., Roberts B., 1993, A&A 273, 642
Joarder P.S., Nakariakov V.M., Roberts B., 1997, Solar Phys. 173, 81
Kippenhahn R., Schlüter R., 1957, Zs. Ap. 43, 36
Kuin N.P.M., Poland A., 1991, ApJ 370, 763
Kuperus M., Raadu M.A., 1974, A&A 31, 189
Lerche I., Low B.C., 1977, Solar Phys. 53, 385
Lerche I., Low B.C., 1980, Solar Phys. 67, 229
Leroy J.L., Bommier V., Sahal-Brechot S., 1984, A&A 131, 33L
Longbottom A.W., Melville J.P., Hood A.W., 1994, Solar Phys. 149, 73
Menzel D., 1951, Proc. Conf. on Dynamics of Ionized Media, London
Milne A.M., Priest E.R., Roberts B., 1979, ApJ 232, 304
Moreno-Insertis F., Schüssler M., Ferriz-Mas A., 1996, A&A 312, 317
Oliver R., Ballester J.L., Hood A.W., Priest E.R., 1993, ApJ 409, 809
Oliver R., Ballester J.L., 1995, ApJ 448, 444
Priest E.R., Hood A.W., Anzer U., 1989, ApJ 344, 1010
Schmitt D., 1995, Habilitationsschrift, Univ. Göttingen
Schmitt D., 1998, Geophys. Astrophys. Fluid Dyn. 89, 75
Schmitt D., Degenhardt U., 1995, Rev. Mod. Astron. 8, 61
Schutgens N.A.J., 1997a, A&A 323, 969
Schutgens N.A.J., 1997b, A&A 325, 352
Spitzer L., 1962, Physics of Fully Ionized Gases. Interscience, New York
Spruit H. C., 1981, A&A 98, 155
Steele C.D.C., Priest E.R., 1990, Solar Phys. 125, 295
Sütterlin P., Wiehr E., Bianda M., Küveler G., 1997, A&A 321, 921
Tandberg-Hanssen E., 1995, The Nature of Solar Prominences. Kluwer
Van der Linden R.A.M., Hood A.W., Goedbloed J.P., 1994, Solar Phys. 154, 69